Solid-State Electronics 198 (2022) 108471

Contents lists available at ScienceDirect

Solid State Electronics

journal homepage: www.elsevier.com/locate/sse

Modeling electrical resistivity of CrSi thin films☆

K. Sonoda [a,*], N. Shiraishi [b], K. Maekawa [a], N. Ito [a], E. Hasegawa [b], T. Ogata [a]

[a] Renesas Electronics Corporation, 751, Horiguchi, Hitachinaka, 312-8511, Ibaraki, Japan
[b] Renesas Electronics Corporation, 1-1-1, Yahata, Minami, 861-4195, Kumamoto, Japan

ARTICLE INFO

Keywords:
Thin film resistor
Chromium silicon
Phase transition
Grain growth
Modeling
Simulation

ABSTRACT

Electrical properties of CrSi thin films are modeled considering phase transitions and grain growth during annealing. The effective medium approximation is used to calculate the electrical resistivity of the film which comprises several phases including grain boundaries. The phase transition from as-deposited amorphous to poly-crystalline including a meta-stable state leads to high resistivity within a certain range of annealing temperature.

1. Introduction

CrSi based thin films are attracting attention because of their high electrical resistivity and low temperature coefficient of resistivity (TCR) [1]. Electrical properties of CrSi thin films depend on microstructure of the constituting materials [2]. Post-annealing changes transport properties because of crystallization [3]. In order to optimize wafer process conditions to achieve desired transport properties, quantitative modeling of the effect of annealing on the electrical properties is required.

In this study, electrical properties of CrSi thin films are modeled considering phase transitions and grain growth during annealing. Experimental data of Cr–Si–C thin films with Si/Cr atomic ratio slightly larger than 2 [2] are used for model validation. The atomic ratio of carbon, which is lower than those of chromium and silicon in the films, is not explicitly included in the formulation of the model for simplicity.

2. Modeling

We formulate the phase transitions during annealing using temperature-dependent transition rates between phases. Volume fractions of each phase are obtained by solving rate equations. The electrical resistivity is calculated based on the volume fractions.

2.1. Phase transitions

The rate equations, which is schematically shown in Fig. 1, are derived based on physical analysis results of the thin films annealed with various temperatures [2]. Scanning transmission electron microscope (STEM) is used to observe microstructure including grain radius. X-ray diffraction (XRD) and nanobeam diffraction (NBD) are used to determine crystal structure. The initial phase, which is labeled as Region 1, is as-deposited amorphous $Cr_{1-x}Si_x$ (a-$Cr_{1-x}Si_x$) with $x = 0.68$. The intermediate phase is polycrystalline Cr_5Si_3 (p-Cr_5Si_3). As the Si/Cr atomic ratio of Cr_5Si_3 is lower than that of the initial a-$Cr_{1-x}Si_x$, the intermediate phase is accompanied by elementary silicon according to the principle of mass-balance. The region including p-Cr_5Si_3 and the elementary silicon is labeled as Region 2. The final phase is polycrystalline $CrSi_2$ (p-$CrSi_2$), which is the stable phase of Cr–Si alloys with Si/Cr atomic ratio around 2 [4,5]. The composition ratios, r_2 and r_3, of the elementary silicon by volume in Regions 2 and 3, respectively, are calculated using the principle of mass-balance with mass numbers (Si: 28, Cr: 52) and mass densities (Si: $2.28\ \mathrm{g/cm^3}$ [6], Cr_5Si_3: $6.05\ \mathrm{g/cm^3}$ [7], $CrSi_2$: $5.02\ \mathrm{g/cm^3}$ [8]).

The rate of Transition $i(=1,2,3)$ shown in Fig. 1 at annealing temperature T_{an} is expressed as

$$P_i = \nu \frac{T_{\mathrm{mp}} - T_{\mathrm{an}}}{T_{\mathrm{mp}}} \exp\left(-\frac{E_{ai}}{kT_{\mathrm{an}}}\right), \tag{1}$$

which is based on the expression for crystal growth [9] with the lattice vibration frequency $\nu = 1 \times 10^{13}$ Hz [10], the melting point $T_{\mathrm{mp}} = 1763$ K [11], and the activation energy E_{ai}.

The volume fractions ϕ_i of Region i is obtained by solving the rate equation

$$\dot{\boldsymbol{\phi}} = \boldsymbol{A}\boldsymbol{\phi}, \tag{2}$$

☆ The review of this paper was arranged by Francisco Gamiz.

* Corresponding author.
E-mail address: kenichiro.sonoda.xc@renesas.com (K. Sonoda).

https://doi.org/10.1016/j.sse.2022.108471

Available online 8 October 2022

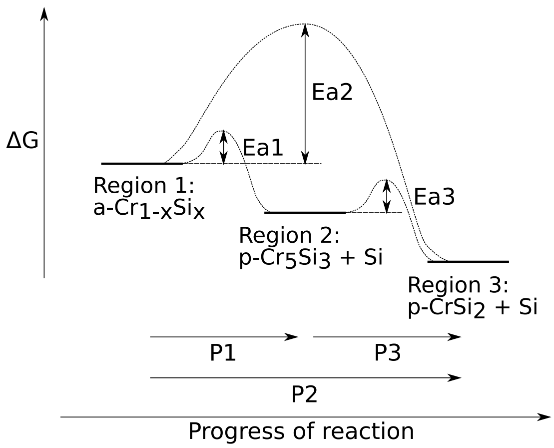

Fig. 1. The schematic diagram of the phase transitions during annealing.

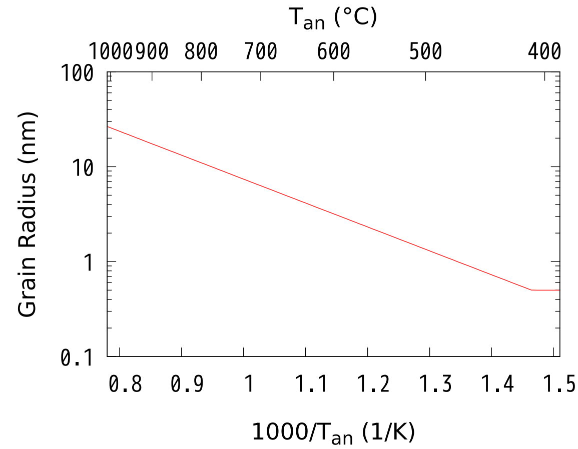

Fig. 2. The grain radius as a function of the annealing temperature. The annealing time is 10 min.

where

$$\boldsymbol{\phi} = \begin{bmatrix} \phi_1 \\ \phi_2 \\ \phi_3 \end{bmatrix}, \tag{3}$$

$$\boldsymbol{A} = \begin{bmatrix} -(P_1+P_2) & 0 & 0 \\ P_1 & -P_3 & 0 \\ P_2 & P_3 & 0 \end{bmatrix}. \tag{4}$$

If the transition rates do not depend on time, the rate equation can be analytically solved as

$$\boldsymbol{\phi}(t) = e^{\boldsymbol{A}t}\boldsymbol{\phi}(0). \tag{5}$$

As the initial phase of the whole system is a-$Cr_{1-x}Si_x$, the initial condition is expressed as

$$\boldsymbol{\phi}(0) = \begin{bmatrix} 1 \\ 0 \\ 0 \end{bmatrix}. \tag{6}$$

The volume fractions of a-$Cr_{1-x}Si_x$, p-Cr_5Si_3, p-$CrSi_2$, and Si are ϕ_1, $(1-r_2)\phi_2$, $(1-r_3)\phi_3$, and $r_2\phi_2 + r_3\phi_3$, respectively.

The physical analysis results also indicate that the higher the annealing temperature, the larger the grains of p-Cr_5Si_3 and p-$CrSi_2$ [2]. Assuming that the grain growth exponent is two [12], the observed grain radius in STEM images after annealing time t_{an} is expressed by

$$r_g = \min\left(k_{gg0}\exp\left(-\frac{E_{agg}}{kT_{an}}\right)t_{an}^{1/2}, r_{gmin}\right) \tag{7}$$

with $k_{gg0} = 1\times10^2$ nm/s$^{1/2}$, $E_{agg} = 0.5$ eV and $r_{gmin} = 0.5$ nm [13] as shown in Fig. 2. The same radius is used for both p-Cr_5Si_3 and p-$CrSi_2$ for simplicity.

2.2. Electrical resistivity

The electrical resistivity of the thin film which comprises a-$Cr_{1-x}Si_x$, p-Cr_5Si_3, p-$CrSi_2$, and Si is calculated using the effective medium approximation [14–16]. In the approximation, the effective conductivity σ_e of the compound which comprises randomly distributed materials A and B with the volume fraction ratio $\eta : 1-\eta$ is given by

$$\eta\frac{\sigma_A - \sigma_e}{\sigma_A + (n-1)\sigma_e} + (1-\eta)\frac{\sigma_B - \sigma_e}{\sigma_B + (n-1)\sigma_e} = 0, \tag{8}$$

where σ_A and σ_B are conductivities of materials A and B, respectively, and n is the dimension of the compound, which is two for thin films. To describe composite materials with more than two components, the iterative method [17] is applied, in which two components are iteratively merged until the whole system is expressed by one effective medium.

Table 1
The resistivity and TCR of each material normalized by the absolute measured values of the as-deposited sample. The grain radius r_g is in nanometers.

Material	Normalized ρ	Normalized TCR
a-$Cr_{1-x}Si_x$	1.09	−0.768
Cr_5Si_3	0.459	12.4
$CrSi_2$	0.725	3.04
Si	19.4	−3.41
grain boundary	$0.258/r_g$	−13.1

In order to include the effect of grain boundary, the resistivity of a polycrystalline material is expressed as a sum of a crystalline part and a grain boundary part: $\rho_p = \rho_c + \rho_{gb}$. According to the Mayadas–Shatzkes (MS) model [18], the grain boundary part ρ_{gb} is described by

$$\frac{\rho_c}{\rho_c + \rho_{gb}} = 3\left[\frac{1}{3} - \frac{\alpha}{2} + \alpha^2 - \alpha^3\log\left(1+\frac{1}{\alpha}\right)\right], \tag{9}$$

where $\alpha = (l_0/d)(R/(1-R))$, l_0 is the background mean free path, d is the average distance between grain boundaries, and R is the reflection coefficient. Assuming $\alpha \ll 1$, $\rho_{gb}/\rho_c \sim (3/2)\alpha = l_1/d$ is obtained, where $l_1 = (3/2)(R/(1-R))l_0$. Considering the distance between grain boundaries are proportional to the grain radius, the grain boundary resistivity ρ_{gb} is inversely proportional to the grain radius. Note that different TCRs are assigned to ρ_c and ρ_{gb} in this study, because the conduction across grain boundaries includes thermally activated process, which is not considered in the derivation of the original MS model. The same grain boundary resistivity is used for both p-Cr_5Si_3 and p-$CrSi_2$ for simplicity.

3. Results and discussion

Activation energies of the transitions and resistivities and TCRs of each material are optimized to minimize the root mean square error between measured and calculated resistivities and TCRs.

The extracted activation energies, E_{a1}, E_{a2}, and E_{a3} are 2.44 eV, 6.36 eV, and 2.52 eV, respectively. Note that these values may depend on atomic ratio of as-deposited films.

The extracted resistivities and TCRs are shown in Table 1. Crystalline Cr_5Si_3 and $CrSi_2$ show relative low resistivity and positive TCR while amorphous $Cr_{1-x}Si_x$ show relative high resistivity and negative TCR, which is known as Mooij correlation [19]. Semiconductor Si shows higher resistivity compared with Cr–Si alloys and negative TCR. The grain boundary shows negative TCR, which suggests that the conduction across grain boundaries includes thermally activated process.

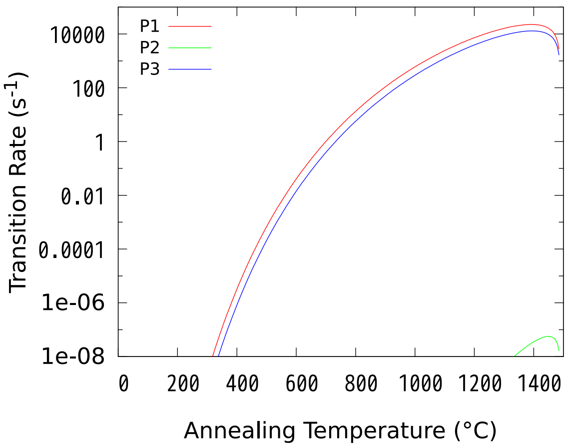

Fig. 3. The temperature dependence of the rate of the transitions shown in Fig. 1.

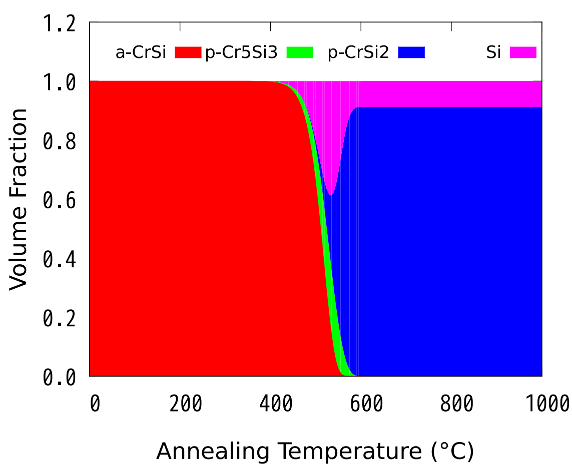

Fig. 4. The volume fraction of each phase. The annealing time is 10 min.

The rate of transitions with the extracted activation energies as shown in Fig. 3 suggests that meta-stable crystals appear first, which is known as Ostwald step rule [20]. The meta-stable state remains within a certain range of annealing temperature around 540 °C as shown in Fig. 4. Note that E_{a1} and E_{a3} are close to the measured activation energy 2.6 eV for silicide formation in multi-layered thin films of chromium and amorphous silicon [21].

Calculated resistivities and the TCRs are in good agreement with measured data as shown in Figs. 5 and 6. The high resistivity within a certain range of annealing temperature around 540 °C can be explain by the Si region which is the residue of the phase transition from as-deposited a-$Cr_{1-x}Si_x$ to meta-stable poly-crystalline Cr_5Si_3. Above 600 °C, the as-deposited a-$Cr_{1-x}Si_x$ is completely transformed to stable poly-crystalline $CrSi_2$ and the resistivity is lower than that of as-deposited a-$Cr_{1-x}Si_x$. The gradual decrease of resistivity and the increase of TCR above 600 °C comes from the grain growth which is shown in Fig. 2. A slight increase in measured resistivity between 600 °C and 700 °C may be attributed to carbon-related phases, which are not considered in our present phase transition model. The relation between the resistivity and the TCR with various annealing temperatures is also well expressed by the proposed model as shown in Fig. 7.

4. Conclusion

The electrical properties of CrSi thin films were modeled considering phase transitions and grain growth during annealing. The phase

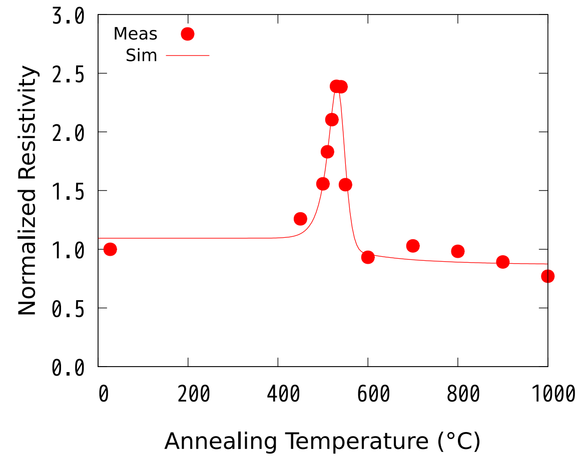

Fig. 5. The resistivity of the thin film as a function the annealing temperature. The resistivity is normalized by the measured value of the as-deposited sample.

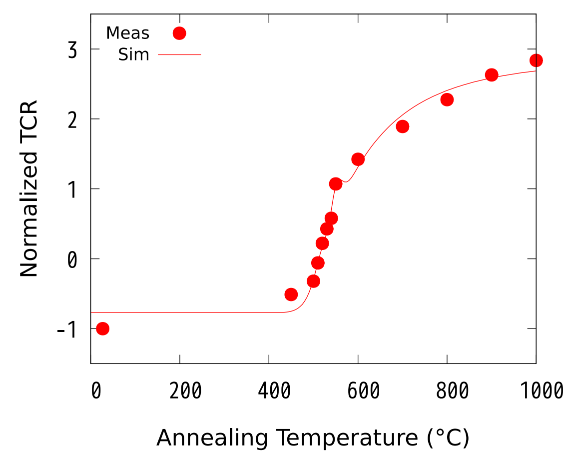

Fig. 6. The TCR of the thin film as a function the annealing temperature. The TCR is normalized by the absolute measured value of the as-deposited sample.

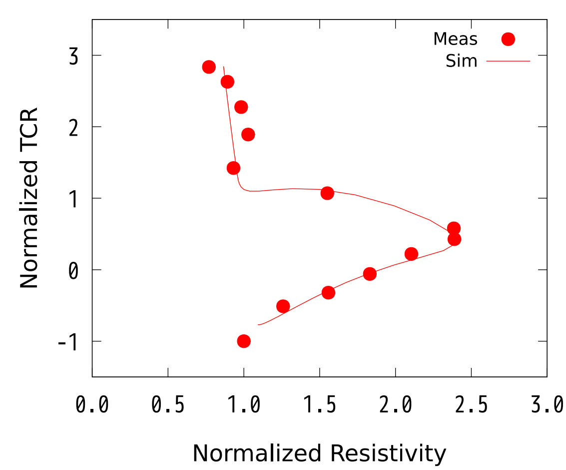

Fig. 7. The dependence of resistivity and TCR on annealing temperature.

transitions from as-deposited amorphous to poly-crystalline including a meta-stable state lead to high resistivity within a certain range of annealing temperature.

Declaration of competing interest

The authors declare that they have no known competing financial interests or personal relationships that could have appeared to influence the work reported in this paper.

Data availability

The data that has been used is confidential.

References

[1] Waits RK. Silicide resistors for integrated circuits. Proc IEEE 1971;59(10):1425–9. http://dx.doi.org/10.1109/PROC.1971.8449.

[2] Ito N, Maekawa K, Kunimune Y, Hasegawa E, Abe K, Shiraishi N, et al. The effect of microstructures on the electrical properties of Cr-Si-C thin film resistors. Japan J Appl Phys 2022. http://dx.doi.org/10.35848/1347-4065/ac6218.

[3] Gladun C, Heinrich A, Schumann J, Pitschke W, Vinzelberg H. Transport properties of nanodisperse Cr_xSi_{1-x} thin films. Int J Electron 1994;77(3):301–8. http://dx.doi.org/10.1080/00207219408926059.

[4] Okamoto H. Cr-Si (chromium-silicon). J Phase Equilib 2001;22(5):593. http://dx.doi.org/10.1361/105497101770332866.

[5] Soleimani-Dorcheh A, Galetz M. Oxidation and nitridation behavior of Cr-Si alloys in air at 1473 K. Oxid Met 2015;84(1):73–90. http://dx.doi.org/10.1007/s11085-015-9544-5.

[6] Mp-149: Si (cubic, Fd-3m, 227). 2022, https://materialsproject.org/materials/mp-149/. [Accessed 16 June 2022].

[7] Mp-7506: Cr5Si3 (tetragonal, I4/mcm, 140). 2022, https://materialsproject.org/materials/mp-7506/. [Accessed 16 June 2022].

[8] Mp-8937: CrSi2 (tetragonal, I4/mmm, 139). 2022, https://materialsproject.org/materials/mp-8937/. [Accessed 16 June 2022].

[9] Redaelli A, Pirovano A, Benvenuti A, Lacaita AL. Threshold switching and phase transition numerical models for phase change memory simulations. J Appl Phys 2008;103(11):6. http://dx.doi.org/10.1063/1.2931951.

[10] Sharma P, Semwal B, Mehrotra K. Vibration spectra and debye temperatures of some transition metals. Z Naturforsch A 1971;26(4):747–52. http://dx.doi.org/10.1515/zna-1971-0418.

[11] Lide DR. CRC handbook of chemistry and physics, Vol. 85. CRC Press; 2004, http://dx.doi.org/10.1021/ja041017a.

[12] Hillert M. On the theory of normal and abnormal grain growth. Acta Metall 1965;13(3):227–38. http://dx.doi.org/10.1016/0001-6160(65)90200-2.

[13] Morales-Rodriguez R. Thermodynamics. Rijeka: IntechOpen; 2012, http://dx.doi.org/10.5772/2615.

[14] Landauer R. The electrical resistance of binary metallic mixtures. J Appl Phys 1952;23(7):779–84. http://dx.doi.org/10.1063/1.1702301.

[15] Khardani M, Bouaïcha M, Bessaïs B. Bruggeman effective medium approach for modelling optical properties of porous silicon: Comparison with experiment. Phys Status Solidi C 2007;4(6):1986–90. http://dx.doi.org/10.1002/pssc.200674420.

[16] Privitera S, Le Neel O, Leung C, Dumont-Girard P, Cialdella B, Bongiorno C, et al. Morphological and electrical characterization of electrically trimmable thin-film resistors. IEEE Trans Electron Devices 2012;59(12):3549–54. http://dx.doi.org/10.1109/TED.2012.2219535.

[17] Nazarov R, Zhang T, Khodzitsky M. Effective medium theory for multi-component materials based on iterative method. In: Photonics, vol. 7, (no. 4):MDPI; 2020, p. 113. http://dx.doi.org/10.3390/photonics7040113.

[18] Mayadas A, Shatzkes M, Janak J. Electrical resistivity model for polycrystalline films: The case of specular reflection at external surfaces. Appl Phys Lett 1969;14(11):345–7. http://dx.doi.org/10.1063/1.1652680.

[19] Mooij J. Electrical conduction in concentrated disordered transition metal alloys. Phys Status Solidi (A) 1973;17(2):521–30. http://dx.doi.org/10.1002/pssa.2210170217.

[20] Van Santen R. The ostwald step rule. J Phys Chem 1984;88(24):5768–9. http://dx.doi.org/10.1021/j150668a002.

[21] Schlesinger T, Cammarata R, Prokes S. Kinetics of silicide formation in chromium-amorphous silicon multilayered films. Appl Phys Lett 1991;59(4):449–51. http://dx.doi.org/10.1063/1.105459.